J. Fluid Mech. (1982), *vol.* 119, *pp.* 475–490
Printed in Great Britain

Bifurcation in steady laminar flow through curved tubes

By K. NANDAKUMAR AND JACOB H. MASLIYAH
Department of Chemical Engineering, University of Alberta,
Edmonton, Alberta, Canada

(Received 10 April 1981 and in revised form 10 December 1981)

The occurrence of dual solutions in curved ducts is investigated through a numerical solution of the Navier–Stokes equations in a bipolar-toroidal co-ordinate system. With the shape of duct being the region formed by the natural co-ordinate surfaces, it was possible to alter the duct geometry gradually and preserve the prevailing form of the velocity field, in a manner suggested by Benjamin (1978).

In addition to the Dean number $Dn = Re/R_c^{\frac{1}{2}}$, a geometrical parameter that defines the shape of the duct was also varied systematically to study the bifurcation of a two-vortex solution into a two- and four-vortex solution. Dual solutions have been found for all geometrical shapes investigated here. Of particular interest are the shapes of a full circle and a semicircle with a curved outer wall.

1. Introduction

Laminar flow in curved ducts has been studied quite extensively for various duct cross-sections. These include circular tubes (Dean 1928; Austin & Seader 1973; Collins & Dennis 1975; Tarbell & Samuels 1973; Van Dyke 1978; Dennis 1980; Lin & Tarbell 1980; Manlapaz & Churchill 1980), elliptical tubes (Cuming 1952), square and rectangular tubes (Cheng & Akiyama 1970; Cheng, Lin & Ou 1976), triangular tubes (Collins & Dennis 1976*a*, *b*), and semicircular ducts (Masliyah & Nandakumar 1979; Masliyah 1980). With the exception of Manlapaz & Churchill (1980), all previous analyses have been limited to coils of zero pitch. In addition, several authors, including Dean (1928), Van Dyke (1978) and Dennis (1980), have used the loose-coiling approximation. This enables the grouping of the two independent parameters, *viz* Reynolds number Re, and the radius of curvature R_c into one single parameter. This parameter has been called the Dean number and defined variously in the literature. We use the definition, $Dn = Re/R_c^{\frac{1}{2}}$. If a numerical procedure is used to solve the equations of motion, as in the present case, no specific advantage is gained by invoking the loose-coiling approximation. Hence the full Navier–Stokes equations will be solved in this work.

The bipolar-toroidal co-ordinate system is shown in figure 1. As long as the zero-pitch approximation is invoked, the equations of motion are invariant to reflection about the (x, y)-plane, indicating a symmetry in the flow pattern.

It has long been established that the laminar flow in curved ducts is composed of a main flow in the axial direction with a superimposed secondary flow having *two* counter-rotating vortices. However, with certain geometries such as square and rectangular ducts (Joseph, Smith & Adler 1975; Cheng *et al.* 1976) or a semicircular duct with a *flat outer wall* (Masliyah 1980) an additional four-vortex secondary flow

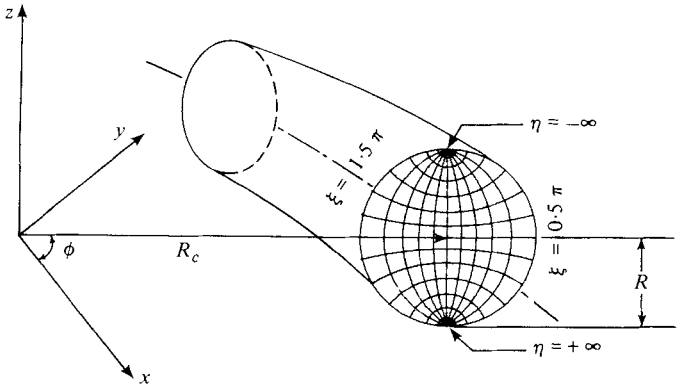

FIGURE 1. Bipolar-toroidal co-ordinate system.

has been predicted. There has been some speculation about the influence of a flat outer wall in producing the additional four-vortex flow pattern (Masliyah 1980).

In spite of considerable effort expended in solving the flow problem in curved *circular* tubes, a four-vortex solution has not been reported until now. It is our understanding that recently Dennis & Ng (1982) and Ng (1980) have been able to obtain a four-vortex flow pattern for a full circle using a series-truncation method. In a recent paper Van Dyke (1978) presented a series solution to the equations of motion in a loosely coiled torus and cast doubt on the accuracy of all previous numerical solutions of Collins & Dennis (1975), Austin & Seader (1973) and Truesdell & Adler (1970). Subsequently Dennis (1980) came to the rescue of earlier numerical solutions by generating accurate solutions using grid-refinement and extrapolation methods. He further suggested that Van Dyke's result could represent a different solution to the problem.

The objective of this work is to study the bifurcation phenomena of flow in coiled tubes and, in particular, flow through tubes with curved outer surfaces. As was pointed out earlier, in addition to a two-vortex solution, a dual four-vortex solution was found to exist for flows in coiled ducts having a flat outer surface. It was hypothesized after Benjamin (1978) that, once a four-vortex dual solution is established, say, for a tube with a flat outer surface, then, using such a solution as an initial one and by gradually changing the geometry of the outer surface from a flat geometry to a circular geometry, it might be possible to conserve a four-vortex solution. In this systematic manner we can establish whether a circular outer geometry will permit the existence of a dual solution having a four-vortex pattern. The bipolar-toroidal co-ordinates used in this study permit such a gradual change in the geometry of the outer surface. Consequently this study deals with the bifurcation phenomena with respect to flow and geometrical parameters.

2. Governing equations

The equations of motion in the stream-function vorticity form for a fully developed viscous flow in a bipolar-toroidal co-ordinate system (η, ξ, ϕ) are given below.

Axial-momentum equation:

$$f_1\left\{\frac{\partial^2 v_\phi}{\partial\eta^2}+\frac{\partial^2 v_\phi}{\partial\xi^2}\right\}-C_1\frac{\partial v_\phi}{\partial\xi}-C_2\frac{\partial v_\phi}{\partial\eta}-C_7 v_\phi=\frac{1}{f_2}Q, \tag{1}$$

where $Q=\partial P/\partial\phi$.

Stream-function vorticity equation:

$$\frac{f_1^3}{f_2}\left\{\frac{\partial^2\psi}{\partial\eta^2}+\frac{\partial^2\psi}{\partial\xi^2}\right\}+C_5\frac{\partial\psi}{\partial\xi}+C_6\frac{\partial\psi}{\partial\eta}=\omega_\phi. \tag{2}$$

Vorticity-transport equation:

$$f_1\left\{\frac{\partial^2\omega_\phi}{\partial\eta^2}+\frac{\partial^2\omega_\phi}{\partial\xi^2}\right\}-C_1\frac{\partial\omega_\phi}{\partial\xi}-C_2\frac{\partial\omega_\phi}{\partial\eta}-C_3\omega_\phi=-C_4 v_\phi. \tag{3}$$

The coefficients are given by

$$f_1=\cosh\eta-\cos\xi,\quad f_2=f_1/[R_c f_1+\sin\xi],$$

$$C_1=v_\xi+\frac{1-\cos\xi\cosh\eta}{f_2},\quad C_2=v_\eta+\frac{\sin\xi\sinh\eta}{f_2},$$

$$C_3=\frac{f_1}{f_2^2}+v_\eta\frac{\sin\xi\sinh\eta}{f_1 f_2}+v_\xi\frac{(1-\cos\xi\cosh\eta)}{f_1 f_2},$$

$$C_4=\frac{2}{f_2}\left[(\sin\xi\sinh\eta)\frac{\partial v_\phi}{\partial\xi}-(1-\cos\xi\cosh\eta)\frac{\partial v_\phi}{\partial\eta}\right],$$

$$C_5=\frac{f_1^2}{f_2^2}(1-\cos\xi\cosh\eta),\quad C_6=\frac{f_1^2}{f_2^2}\sin\xi\sinh\eta,$$

$$C_7=\frac{f_1}{f_2^2}-v_\eta\frac{\sin\xi\sinh\eta}{f_1 f_2}-v_\xi\frac{1-\cos\xi\cosh\eta}{f_1 f_2}.$$

The metric coefficients for the bipolar-toroidal co-ordinate system are

$$h_\xi=h_\eta=\cosh\eta-\cos\xi, \tag{4}$$

$$h_\phi=\frac{\cosh\eta-\cos\xi}{R_c(\cosh\eta-\cos\xi)+\sin\xi}. \tag{5}$$

The equations were rendered dimensionless as follows:

$$R_c=\frac{R_c'}{R'},\quad \mathbf{v}=\frac{\mathbf{v}'}{\nu/R'},\quad Q=\frac{R'^2}{\nu\mu}\frac{\partial p'}{\partial\phi},$$

$$\psi=\frac{\psi'}{\nu R'},\quad \omega_\phi=\frac{\omega_\phi'}{\nu/R'^2},\quad P=\frac{p'}{\mu\nu/R'^2}.$$

The prime denotes a dimensional quantity, and R' is the radius of the duct measured along $\xi=\pi$ and R_c' is the radius of curvature.

The secondary velocities v_ξ and v_η are given by

$$v_\eta=-\frac{f_1^2}{f_2}\frac{\partial\psi}{\partial\xi}, \tag{6}$$

$$v_\xi=\frac{f_1^2}{f_2}\frac{\partial\psi}{\partial\eta}, \tag{7}$$

and the axial vorticity is given by

$$\omega_\phi = f_1^2\left\{\frac{\partial}{\partial\eta}\frac{v_\xi}{f_1} - \frac{\partial}{\partial\xi}\frac{v_\eta}{f_1}\right\}. \tag{8}$$

Because of symmetry about the co-ordinate $\eta = 0$ only the half-region $\eta \in [0, \infty]$ will be considered. The transformation

$$\eta = \tfrac{1}{2}(e^\beta - 1) \tag{9}$$

has been found to be useful in providing more grid points near the co-ordinate $\eta = 0$.

The boundary conditions are

(*a*) *axial velocity:*

$$v_\phi = 0 \quad \text{on wall,} \tag{10}$$

$$\frac{\partial v_\phi}{\partial\eta} = 0 \quad \text{along} \quad \eta = 0 \quad \text{(symmetry);} \tag{11}$$

(*b*) *stream function:*

$$\psi = 0 \quad \text{on all boundaries;} \tag{12}$$

(*c*) *vorticity:*

$$\omega_\phi = 0 \qquad \text{along} \quad \eta = 0, \tag{13}$$

$$\omega_\phi = \frac{f_1^3}{f_2}\frac{\partial^2\psi}{\partial\xi^2} \quad \text{along} \quad \xi = \text{constant}, \tag{14}$$

$$\omega_\phi = \frac{f_1^3}{f_2}\frac{\partial^2\psi}{\partial\eta^2} \quad \text{along} \quad \eta = \text{constant}. \tag{15}$$

The friction coefficient C_f is defined as

$$C_f = \frac{\langle\tau'_w\rangle}{\frac{1}{2}\rho\langle v'_\phi\rangle^2}, \tag{16}$$

and is computed from

$$C_f = 2D_e(-Q)\frac{A_x}{A_w}\frac{1}{\langle v_\phi\rangle}\frac{1}{Re} \tag{17}$$

where $D_e = 4V_w/A_w$ is the equivalent diameter, A_x is the cross-sectional flow area, A_w is the wetted wall-surface area/unit ϕ, V_w is the wetted volume/unit ϕ,

$$Re = D'_c\langle v'_\phi\rangle/\nu = D_e\langle v_\phi\rangle, \tag{18}$$

and τ'_w is the wall shear stress.

The pressure gradient along the equator ($\eta = 0$) of the tube can be deduced from the ξ-direction of the Navier–Stokes equation to give

$$\frac{\partial P}{\partial\xi} = 2\frac{\partial\omega_\phi}{\partial\beta} - \frac{1}{2}\frac{\partial v_\xi^2}{\partial\xi} - \frac{v_\phi^2}{R_c(1-\cos\xi)+\sin\xi},$$

with all quantities evaluated at $\eta = \beta = 0$. Integration of the above equation along ξ gives

$$(P - P_i)_{\eta=0} = -2\int_\xi^{\xi_i}\frac{\partial\omega_\phi}{\partial\beta}d\xi - \tfrac{1}{2}v_\xi^2 + \int_\xi^{\xi_i}\frac{v_\phi^2\,d\xi}{R_c(1-\cos\xi)+\sin\xi}, \tag{19}$$

where ξ_i is the value of ξ at the inner surface. P and P_i are the pressures at ξ and at the inner surface respectively. The pressure gradient along the tube surface is given by

$$2e^{-\beta}\frac{\partial P}{\partial\beta} = \left[-\frac{\partial\omega_\phi}{\partial\xi} + \frac{\omega_\phi(\sin\xi - f_1\cos\xi)}{f_1(R_c f_1 + \sin\xi)}\right]_{\xi=\xi_i \text{ or } \xi_o} \tag{20}$$

R_c	$-Q$	Shape	Present study $C_f Re$	Previous study $C_f Re$	Difference %	Reference
10000	—	Full circle, two vortex	16·07	16·0	0·45	—
100	600000	Full circle, two vortex	24·05	23·92	0·54	Austin & Seader (1973)
10	24000	Full circle, two vortex	26·11	26·192	0·25	Tarbell & Samuels (1973)
100	1060000	Full circle, four-vortex	27·41	27·26	0·54	Dennis & Ng (1982)
30	400000	Semicircle, two-vortex	20·88	20·89	0·05	Masliyah & Nandakumar (1979)
100	707107	Full circle, two-vortex	25·21	24·736	1·9	Dennis (1980, 1981)

TABLE 1. Comparison with other solutions (present solutions with 21 × 21 grid)

(ξ_0 is the value of ξ at the outer surface). When the radius of curvature R_c is large the second term on the right-hand side of (20) becomes negligible.

3. Method and accuracy of solution

The governing partial differential equations (1)–(3) were discretized using central-difference approximations. The resulting algebraic equations were solved using the multigrid method. The details of the solution procedure could be found in Nandakumar & Masliyah (1981) and Brandt (1980).

The bipolar co-ordinates are such that a semi-infinite domain must be spanned in the η-co-ordinate direction. But the finite-difference method requires the selection of a finite domain. Choosing $\beta = 3{\cdot}0$ ($\eta = 9{\cdot}5428$) spans most of the physical space with $z = 0{\cdot}99986$ (as opposed to the exact value of 1·0). The region enclosed by the co-ordinates $\eta \in [0, 9{\cdot}5428]$ and $\xi \in [0{\cdot}5\pi, 1{\cdot}5\pi]$ corresponds to a full circle, and choosing $R_c = 10000$ simulates a straight circular tube. For this case the product $C_f Re$ was 16·07 with a grid size of 21 × 21, which is within 0·45 % of the exact value of 16. Five more examples, representing a variety of cases such as full and semicircles, two- and four-vortex solutions, are compared with the literature values in table 1. In all cases the present solution agrees with the established values within 2 %. As a further check on the accuracy of the numerical solution, the total shear force was evaluated by integrating the wall shear stress $\tau_{\xi\phi}$ and $\tau_{\eta\phi}$. The friction coefficient was subsequently computed from

$$C_f = 2\langle \tau_w \rangle D_e / \langle v_\phi \rangle Re. \tag{21}$$

The difference in the friction coefficient computed from (17) and (21) was on the average about 3 %.

4. Results and discussion

All the earlier workers studying the flow in curved circular and semicircular ducts have preferred the cylindrical-toroidal (i.e. (r, θ, ϕ)) co-ordinate system. Using this co-ordinate system, Masliyah (1980) obtained dual solutions in a semicircular duct

with a *flat outer wall*. Using the same co-ordinate system Masliyah & Nandakumar (1979) failed to obtain a dual solution for a semicircular duct with a *curved outer wall*. The cylindrical co-ordinate system (r, θ) does not permit the geometry to be changed gradually from a semicircle to a full circle and *vice versa*. The four-vortex solution found in a semicircle with a flat outer wall is not preserved when the geometry is changed abruptly to a full circle. However, in a bipolar co-ordinate system semicircular and circular geometries are obtained as special cases, and in addition it is possible to make a gradual change from one geometry to the other.

Inspired by the work of Benjamin (1978), who studied bifurcation of Taylor vortices with respect to a geometrical parameter and a flow parameter, the present problem was formulated in a similar manner. The state function characterizing a solution was chosen as $C_f R_c^{\frac{1}{2}}$. The geometrical parameter was chosen as the co-ordinate values of the inner (ξ_i) and outer (ξ_o) surfaces of the duct in a bipolar co-ordinate system. The Dean number was used as the flow parameter.

A semicircular duct with a flat outer wall was considered first, because Masliyah (1980) found that it was fairly easy to establish the dual solution for this geometry. Starting from a converged two-vortex solution, the four-vortex solution was obtained by perturbing the flow significantly (i.e. by increasing the Dean number by a large amount). The four-vortex solution was then preserved by *gradually* changing either the Dean number or the shape of the inner and/or outer surfaces of the duct.

The state function $C_f R_c^{\frac{1}{2}}$ is shown as a function of ξ_o and Dn in figure 2. The radius of curvature R_c was chosen as 30 for all cases. The inner wall of the duct was chosen as a semicircle (i.e. $\xi_i = 1{\cdot}5\pi$). The shape of the outer wall was changed gradually through several moon-shaped configurations ($\xi_o = 1{\cdot}05\pi, \pi, 0{\cdot}75\pi, 0{\cdot}6\pi$) to a full circle ($\xi_o = 0{\cdot}5\pi$). For each fixed outer configuration, the Dean number was varied up to 170 in order to generate the surface of the state function. In all cases a two-vortex solution was found to bifurcate into a two- and four-vortex solution above a Dean number of about 100. Hence it is clear that the shape of the outer wall does not play a crucial role in determining the type of solution. It does, however, play a role in determining the region of attraction of the four-vortex solution. It was much easier to obtain the four-vortex solution when the outer surface was almost flat. The difference in the value of the state function for the two- and four-vortex solutions diminishes with decreasing ξ_o. It appears that the region of attraction of the four-vortex solution decreases as the outer surface becomes curved. Hence, starting from a converged solution on the four-vortex surface in figure 2, the change in ξ_o or Dn must be small enough to obtain yet another converged solution on the same surface; otherwise the solution jumps to the two-vortex surface.

Another interesting feature of figure 2 is the crossover of the two surfaces in the range $0{\cdot}6\pi > \xi_o > 0{\cdot}5\pi$. Since this is a numerical study it is not possible to analyse the nature of this critical curve. But there is no doubt that the four-vortex surface is above the two-vortex one for $\xi_o > 0{\cdot}6\pi$. This is in agreement with Masliyah (1980) for $\xi_o = \pi$. For the full circle (i.e. $\xi_o = 0{\cdot}5\pi$) the friction coefficient for the four-vortex solution is smaller than that for the two-vortex solution. The analysis of Dennis & Ng (1982) also indicates that, using an entirely different numerical procedure, a similar pattern emerges for the full circle.

Having established a four-vortex solution for the full circle through gradual changes in ξ_o, it is now possible to study the effect of the radius of curvature. However, the

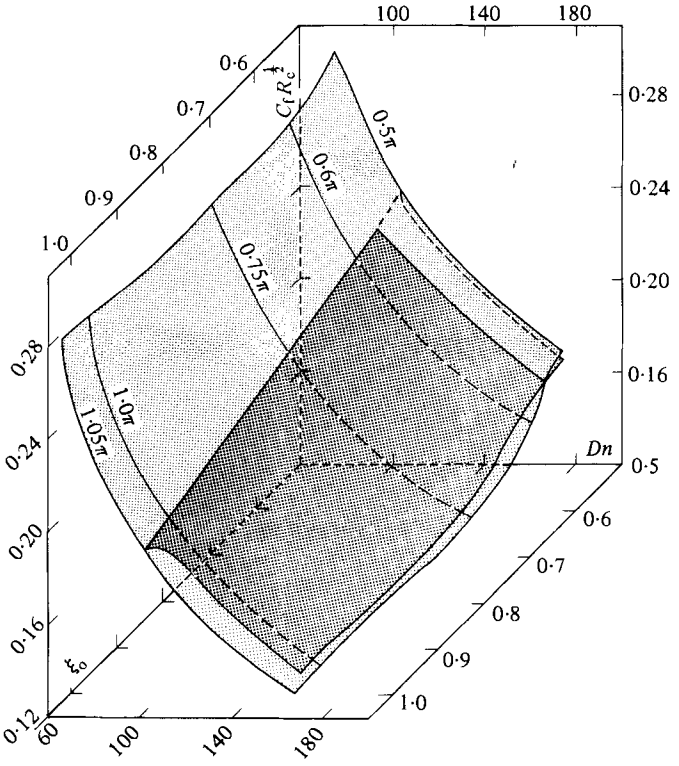

FIGURE 2. State-function variation with Dean number and outer surface geometry.

		Two-vortex solution		Four-vortex solution	
R_c	$-Q$	Dn	$C_f Re$	Dn	$C_f Re$
100	500000	86·73	23·07	No solution	
100	600000	99·82	24·05	No solution	
100	700000	112·2	24·97	113·6	24·65
100	800000	—	—	124·0	25·82
100	900000	—	—	137·0	26·28
100	1060000	—	—	154·8	27·41
60	300000	—	—	106·7	24·20
30	100000	99·88	24·38	No solution	
30	117000	112·40	25·35	113·3	25·15
30	125000	118·0	25·80	119·1	25·56
30	150000	134·4	27·18	136·9	26·68
30	200000	162·6	29·96	170·0	28·66
20	80000	—	—	134·3	26·65
15	70000	—	—	166·2	29·00
10	24000	116·3	26·11	117·4	25·86
10	30000	136·9	27·73	138·5	27·40
10	35000	—	—	155·3	28·51
10	50000	—	—	201·7	31·30

TABLE 2. Computed results for full circle, $\xi \in \lfloor 0{\cdot}5\pi, 1{\cdot}5\pi]$

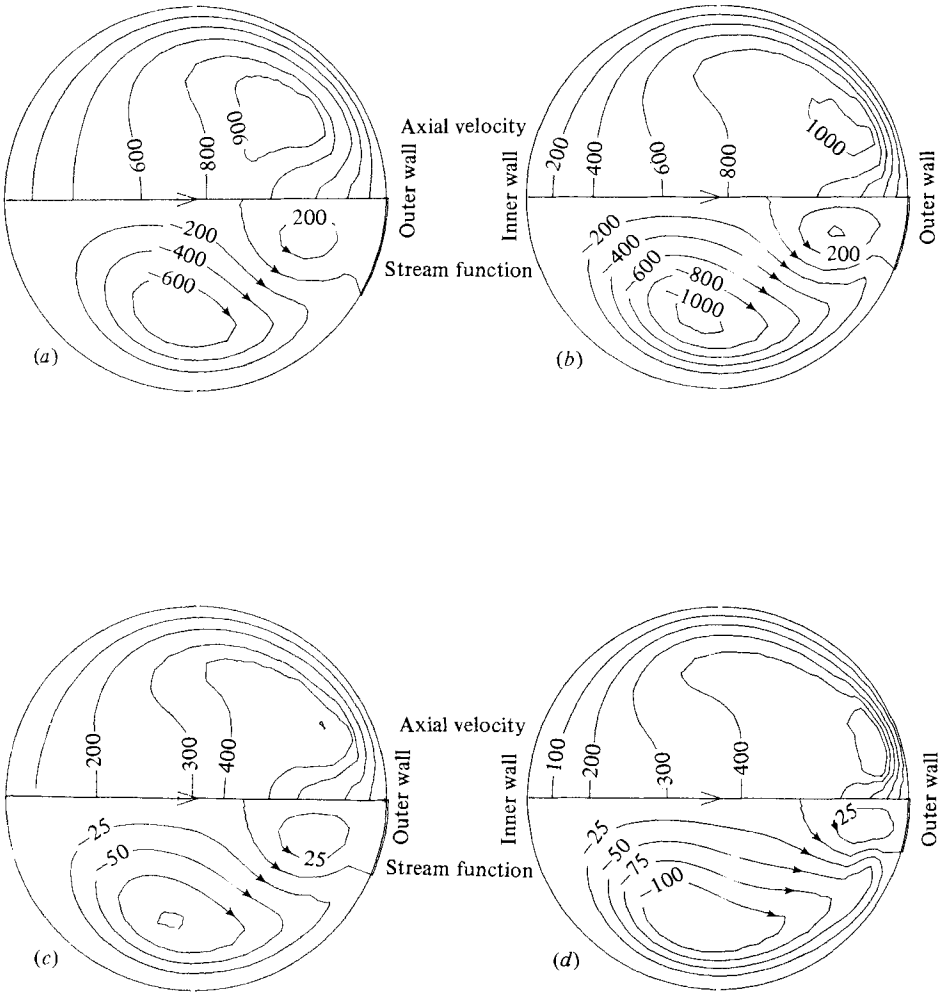

FIGURE 3. Contours of stream function and axial velocity for a full circle: (*a*) $R_c = 100$, $Dn = 113{\cdot}6$; (*b*) 100, 154·8; (*c*) 10, 155·3; (*d*) 10, 201·7.

	Two-vortex solution		Four-vortex solution	
$-Q$	Dn	$C_f Re$	Dn	$C_f Re$
150000	46·63	17·68	No solution	
250000	71·75	19·14	No solution	
400000	105·3	20·88	—	—
460000	—	—	117·6	21·50
500000	125·9	21·83	125·0	21·99
550000	135·8	22·26	135·0	22·39
700000	163·15	23·47	164·0	23·46
900000	197·74	25·00	199·4	24·80
1200000	—	—	249·8	26·40

TABLE 3. Computed results for semicircle, $\xi \in [0{\cdot}5\pi, \pi]$ (curved outer surface)

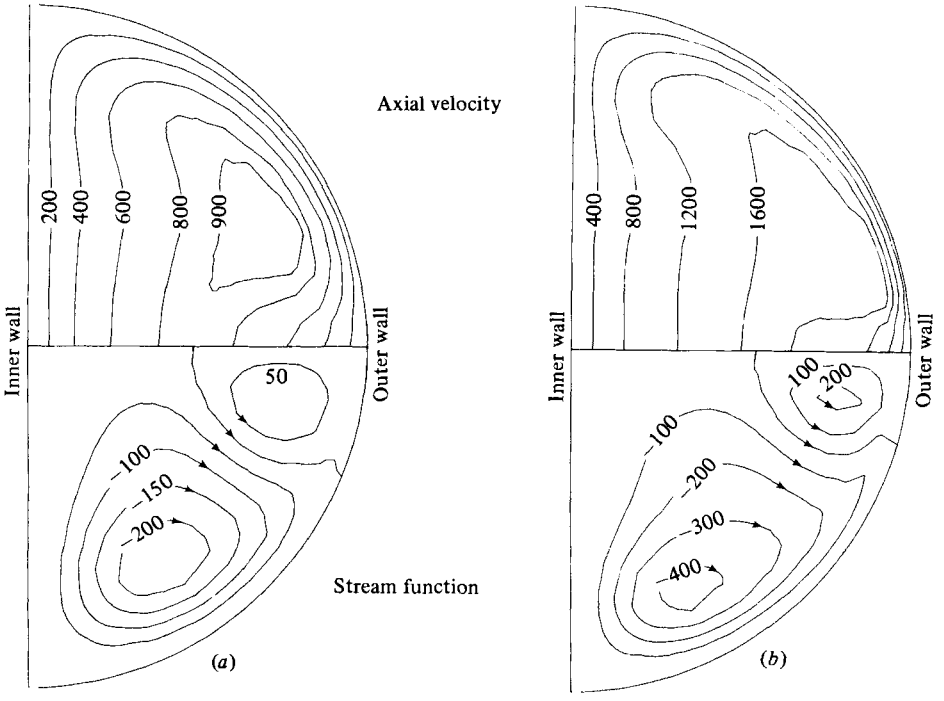

FIGURE 4. Contours of stream function and axial velocity for a semicircle with a curved outer wall: (*a*) $R_c = 30$, $Dn = 125{\cdot}0$; (*b*) 30, 249·8.

changes in R_c must be gradual to retain a four-vortex solution. For example, starting with a four-vortex solution for $R_c = 30$ and changing to $R_c = 10$ in one step causes the solution to converge to a two-vortex one. To retain the four-vortex pattern R_c had to be changed in steps as 30, 20, 15 and 10. Computed results are shown in table 2 for $R_c = 100$, 30, 10. To aid in flow visualization, the contours of stream function and axial velocity are shown in figure 3 for four cases. Only the four-vortex patterns are presented. The size of the secondary vortex in a full circle is small compared to the flow area, and the flow in the left half of the duct is basically the same as in a two-vortex pattern. This is perhaps the reason for the smaller difference in the state function $C_f R_c^{\frac{1}{2}}$ for the two solutions. For a chosen R_c, increasing Dn (through Q) appears to reduce the size of the secondary vortex. This is more pronounced for the case of $R_c = 10$.

Starting from a converged four-vortex solution for a full circle, and keeping the shape of the outer wall as a semicircle ($\xi_o = 0{\cdot}5\pi$), the inner wall was gradually changed from $1{\cdot}5\pi$ through $1{\cdot}4\pi$, $1{\cdot}25\pi$, $1{\cdot}1\pi$ to $1{\cdot}0\pi$. In all cases a converged four-vortex solution was obtained. The final geometry ($\xi_i = \pi$, $\xi_o = 0{\cdot}5\,\pi$) corresponds to a semicircle with a flat inner wall and a curved outer wall, a case studied by Masliyah & Nandakumar (1979). After establishing a four-vortex solution for this geometry, the flow parameter was varied, and the computed results are shown in table 3. For this geometry, the difference in $C_f Re$ between the two- and four-vortex solution is even smaller. The contours of stream function and axial velocity, shown in figure 4, are similar to the other four-vortex solutions presented earlier.

Figures 5–10 show some detail of the flow field for the case of a full circle. For the

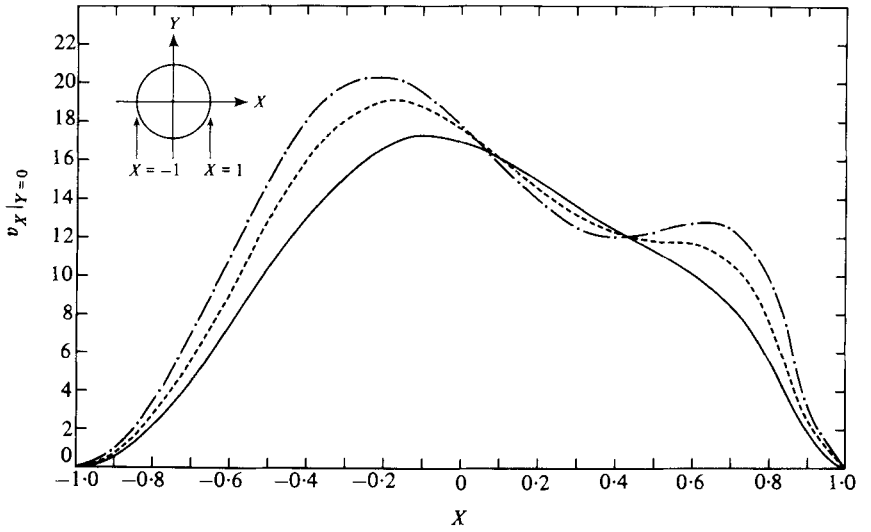

FIGURE 5. Variation of the radial velocity along the equator for a full circle with $R_c = 30$. Two-vortex solution: ——, $Dn = 84$; – – –, 112·4; – · – · – ·, 134·4.

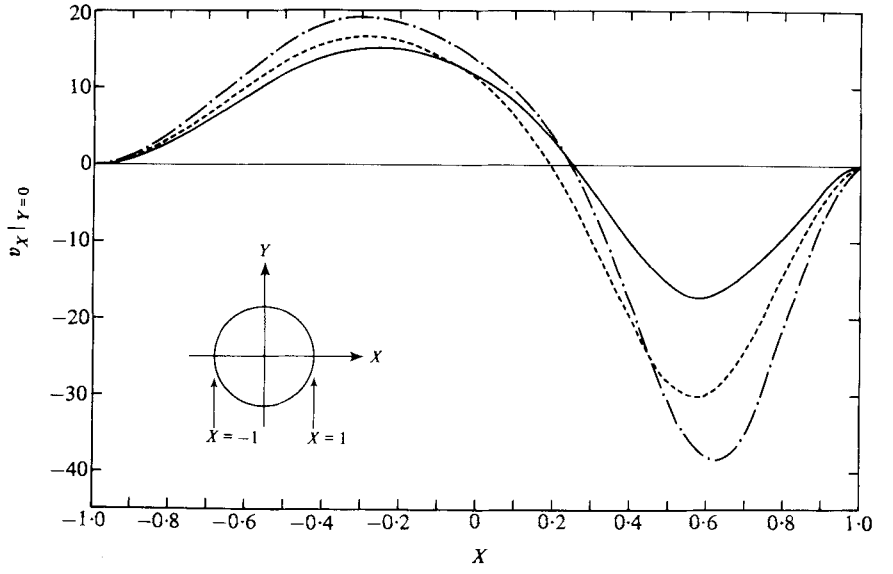

FIGURE 6. Variation of the radial velocity along the equator for a full circle with $R_c = 30$. Four-vortex solution: ——, $Dn = 113{\cdot}3$; – – –, 136·9; – · – · – ·, 170.

case of two-vortex solutions, figure 5 shows that there exists a region between the tube centre and the outer surface ($0 < X < 0{\cdot}4$) where the radial velocity along the tube equator decreases as it approaches the outer surface. In this region, there also exists an adverse pressure gradient (figure 9). This is a flow situation inducive to separation, and indeed figure 6 shows that radial flow reversal, a change in the sign of v_X, occurs for the four-vortex solution in the region where the two-vortex solution has a decreasing velocity and an adverse pressure gradient.

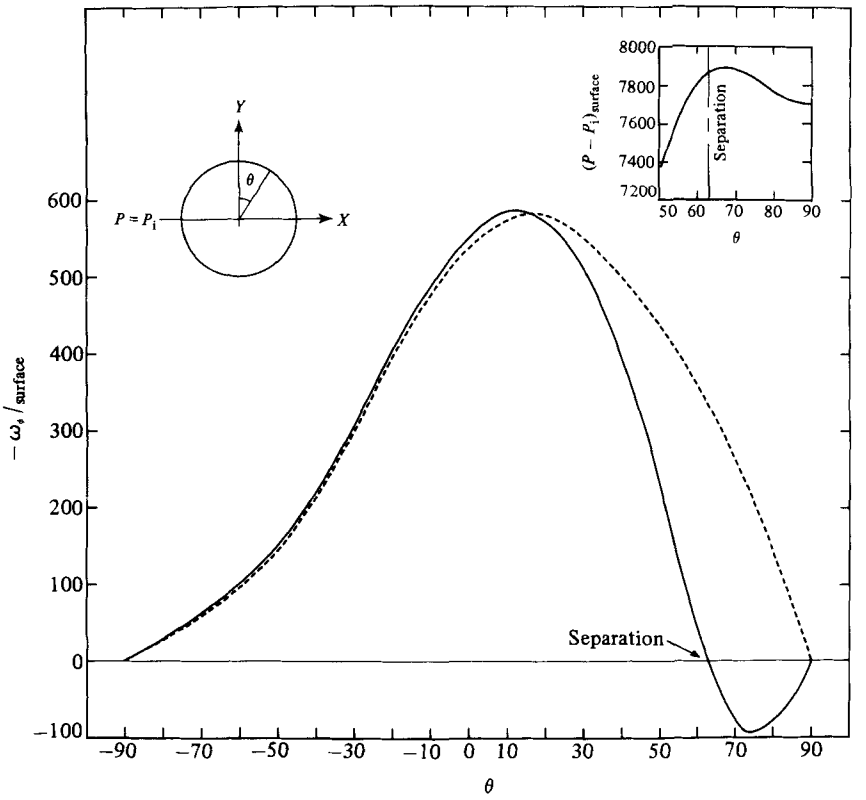

FIGURE 7. Variation of surface vorticity for a full circle with $R_c = 30$, $Q = -117000$: - - - -, two-vortex solution; ——, four-vortex solution.

The radial velocity $v_X(=-v_\xi)$ along the line of symmetry, $\eta = Y = 0$, is shown in figure 6 for the case of four-vortex solutions. The radial velocity in the secondary vortex can be seen to be fairly large compared with that in the primary vortex. For a Dean number of 113·3 the maximum values of the radial velocity in the primary and in the secondary vortices are of similar magnitude. For the case of the higher Dean number of 170 the value of the radial velocity in the secondary vortex is about double that in the primary vortex. This indicates that the circulation in the secondary vortex is fairly intense. Examination of the contours of the stream function for curved rectangular channels with secondary vortices (De Vriend 1981) also indicates that the radial velocity in the secondary vortex along the symmetry line can be higher than that in the primary vortex.

Variation of the surface vorticity $-\omega_\phi$ is shown in figure 7. The surface vorticities for the two types of solution show very close agreement over a large portion of the tube surface, and only differ in the region close to the outer surface.

The point of reattachment to the tube surface of the zero streamline that separates the primary and the secondary vortices is the point of separation of the secondary-flow boundary layer. This separation point is characterized by a zero surface shear stress $\tau_{\xi\eta}$, which is given by the vorticity ω_ϕ at the surface. Consequently the location of the change in sign of the surface vorticity can be used to locate the separation point at the tube surface. For the case of $Dn = 113{\cdot}3$ shown in figure 7 the change in the

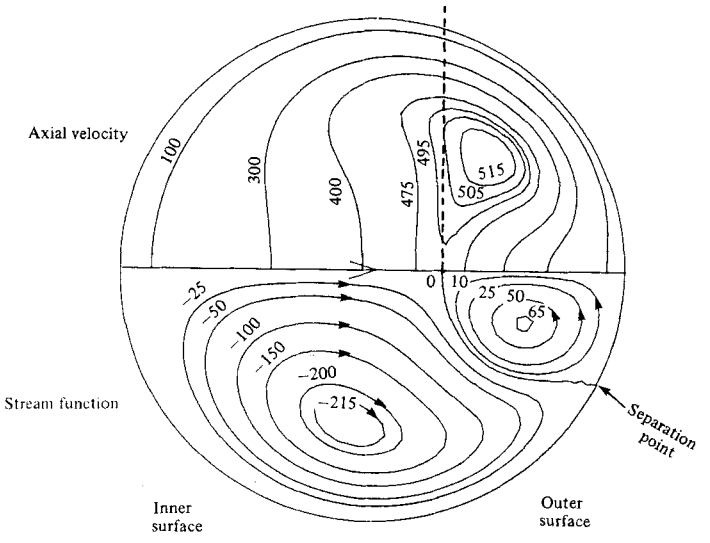

FIGURE 8. Contours of stream function and axial velocity for a full circle with $R_c = 30$, $Q = -117000$, $Dn = 113{\cdot}3$.

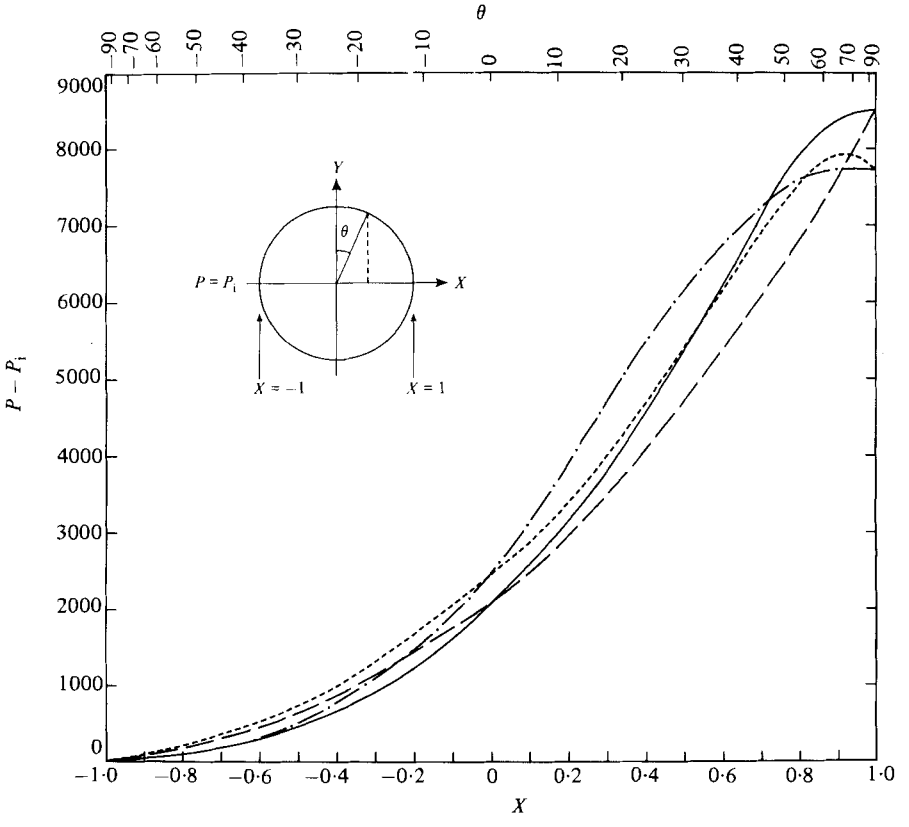

FIGURE 9. Variation of the pressure drop along the equator and the circumference for the case of a full circle with $R_c = 30$, $Q = -117000$. Two-vortex solution: ——, equator; — —, circumference. Four-vortex solution: – · – · –, equator, - - - -, circumference.

sign of the surface vorticity occurs at $\theta = 63°$. This value is confirmed from a streamline contour plot shown in figure 8, which was produced from a 41×41 grid. The general features of figure 8 are completely consistent with those of Dennis & Ng (1982).

Figure 9 shows the pressure drops along the tube equator and along the tube circumference, evaluated using (19) and (20) respectively. The pressure difference between the outer and the inner surfaces for the case of the four-vortex solution is lower than that for the case of the two-vortex solution. For a given type of solution and at a constant value of X, the pressure values at the equator and at the circumference differ little from each other in the region of $-1 < X < 0$. Also, in the region $-1 < X < 0$ the pressure variation along the equator is fairly similar for both types of solutions. However, along the tube circumference near the region of the outer surface there is a striking difference in the pressure variation between the two types of solution. For the case of the four-vortex solution the pressure exhibits a maximum in the region of the secondary vortex. This maximum occurs at $\theta = 67°$, as indicated by the upper horizontal axis of figure 9 and the supplementary pressure-variation plot of figure 7. For the flow situation presented here a zero surface pressure gradient occurs after separation has taken place, and the separation occurs within the region of a positive pressure gradient. This is in accordance with boundary-layer separation for flow past non-flat surfaces.

From figures 3 and 4 of this paper and from the work of Masliyah (1980) and Cheng *et al.* (1976) the flow profile around the stagnation point appears to have a unique character irrespective of the geometry. Ignoring the minor fluctuations of the contour lines due to the contouring subroutines, the stream-function contour separating the two sets of vortices appears to intersect the line of symmetry ($\eta = 0$) at right angles. Close to the stagnation point an expansion for the stream function in terms of $[(X - X_s), Y]$ up to order 3, and consistent with the conditions

$$\psi(X, Y = 0) = 0,$$

$$v_X(X_s, 0) = \left.\frac{\partial \psi}{\partial Y}\right|_{X_s, 0} = 0,$$

$$\frac{\partial v_X}{\partial Y} = \left.\frac{\partial^2 \psi}{\partial Y^2}\right|_{X, Y=0} = 0,$$

$$v_Y(X, Y = 0) = \left.\frac{\partial \psi}{\partial X}\right|_{X, Y=0} = 0,$$

can be written as

$$\psi(X, Y) = -aY(X - X_s) + bY^3 + cY(X - X_s)^2, \tag{22}$$

with $a, b, c > 0$, and where v_X, v_Y are the velocities in the X- and Y-directions respectively. The (X, Y)-co-ordinate system has its origin at the tube centre. The symbol X_s is the value of X at the stagnation point, which is defined by the location of the intersection of the dividing streamline with the line of symmetry. Equation (22) gives the dividing streamline as

$$Y = \left[\frac{a(X - X_s) - c(X - X_s)^2}{b}\right]^{\frac{1}{2}}, \tag{23}$$

which clearly intersects the line of symmetry at right angles. Equation (23) can be further simplified by neglecting the second-order effects represented by the second term.

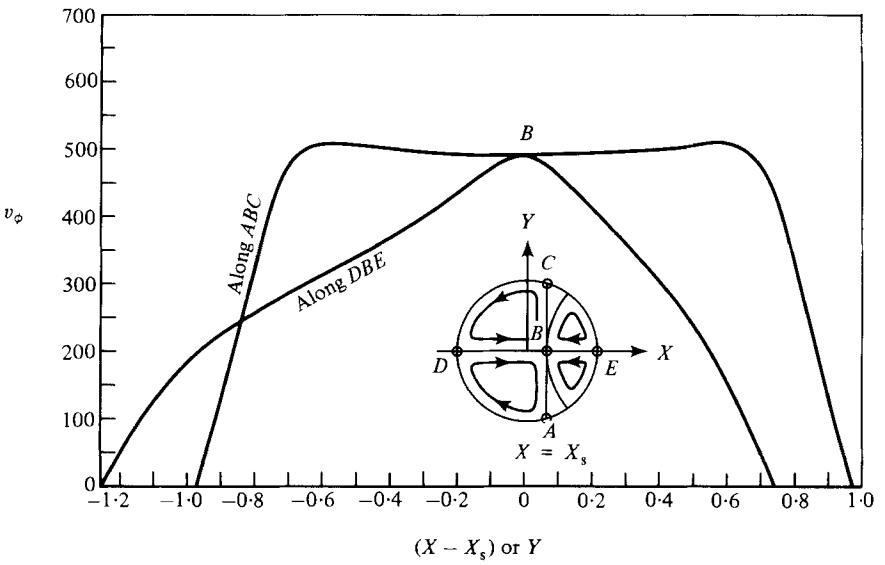

FIGURE 10. Variation of the axial velocity along the equator and along Y, $X = X_s$ for a full circle with $R_c = 30$, $Q = -117\,000$, $Dn = 113{\cdot}3$.

When (22) is used in the secondary-flow momentum equation in the Cartesian toroidal form (Cheng & Akiyama 1970) we can deduce that at $(X_s, 0)$, $\partial v_\phi/\partial Y = 0$ and that $\partial^2 v_\phi/\partial Y^2 > 0$. Hence the velocity profile in the direction perpendicular to the line of symmetry passing through the stagnation point passes through a minimum. Further, from the axial-momentum equation at the stagnation point we can deduce that $\partial^2 v_\phi/\partial X^2 < 0$. At this point we are not able to ascertain the magnitude of $\partial v_\phi/\partial X$ using the Navier–Stokes equation, and hence the nature of axial velocity about the stagnation point along the equator. However, as the magnitude of the secondary velocities is much smaller than the axial velocity around the stagnation point, we can expect that for at least *low-Dean-number* flow situations the axial velocity would be locally Poiseuille, and an expansion of the form

$$v_\phi(X, Y) = v_\phi(X_s, 0)\,[1 - d(X - X_s)^2 + eY^2 + \ldots], \tag{24}$$

where $d > 0$ and $e > 0$, would be appropriate. The signs of the coefficients are determined from the fact that $\partial^2 v_\phi/\partial X^2 < 0$ and $\partial^2 v_\phi/\partial Y^2 > 0$ at the stagnation point $X = X_s$. The axial velocity near the stagnation point described by (24) is the shape of a saddle. Figure 10 shows the variation of the axial velocity along the tube equator and along a line perpendicular to the equator through the stagnation point for a Dean number of 113·3 and $R_c = 30$. The axial-velocity profile around the stagnation point is clearly that of a saddle point, as predicted by the analysis outlined above. A contour plot for the axial velocity and stream function is shown in figure 8 for the same Dn and R_c values. This plot also shows fairly clearly that at the stagnation point the axial velocity exhibits a maxima along the line of symmetry and a minimum along $X = X_c$ (dotted line). Close examination of the flow contours of figures 3 and 4 also indicates that the stagnation point on the line of symmetry is also a saddle point of v_ϕ for lower values of R_c and for a different flow geometry. The axial velocity along $Y, X = X_s$ of figure 10 was obtained using two-dimensional Laplacian–spline interpolation.

6. Conclusions

Through the use of bipolar-toroidal co-ordinates it was possible to show that for flow in helical tubes flow bifurcation exists irrespective of the shape of the tube. However, it is much easier to obtain a dual solution when the outer surface is nearly flat. For the four-vortex solutions, the stagnation point on the line of symmetry is a saddle point of the axial velocity.

The authors wish to thank the University of Alberta for the use of computer facilities, and the Natural Sciences and Engineering Research Council of Canada for financial support. The authors also wish to thank one of the referees for pointing out the existence of the saddle point in the axial velocity.

REFERENCES

AUSTIN, L. R. & SEADER, J. D. 1973 Fully developed viscous flow in coiled circular pipes. *A.I.Ch.E. J.* **19**, 85–94.

BENJAMIN, T. B. 1978 Bifurcation phenomena in steady flows of a viscous fluid. I. Theory. *Proc. R. Soc. Lond.* A **359**, 1–26; II. Experiments. *Proc. R. Soc. Lond.* A **359**, 27–43.

BRANDT, A. 1980 Multilevel adaptive computations in fluid dynamics. *A.I.A.A. J.* **18**, 1165–1172.

CHENG, K. C. & AKIYAMA, M. 1970 Laminar forced convection heat transfer in curved rectangular channels. *Int. J. Heat Mass Transfer* **13**, 471–490.

CHENG, K. C., LIN, R.-C. & OU, J.-W. 1976 Fully developed laminar flow in curved rectangular channels. *Trans. A.S.M.E.I., J. Fluids Engng* **98**, 41–48.

COLLINS, W. M. & DENNIS, S. C. R. 1975 The steady motion of a viscous fluid in a curved tube. *Quart. J. Mech. Appl. Math.* **28**, 133–156.

COLLINS, W. M. & DENNIS, S. C. R. 1976*a* Viscous eddies near a 90° and a 45° corner in flow through a curved tube of triangular cross-section. *J. Fluid Mech.* **76**, 417–432.

COLLINS, W. M. & DENNIS, S. C. R. 1976*b* Steady flow in a curved tube of triangular cross section. *Proc. R. Soc. Lond.* A **352**, 189–211.

CUMING, H. G. 1952 The secondary flow in curved pipes. *Aero. Res. Counc. R. & M.* no. 2880.

DEAN, W. R. 1928 The stream-line motion of fluid in a curved pipe. *Phil. Mag.* **5**(7), 673–695.

DENNIS, S. C. R. 1980 Calculation of the steady flow through a curved tube using a new finite-difference method. *J. Fluid Mech.* **99**, 449–467.

DENNIS, S. C. R. & NG, M. C. 1982 Dual solution for steady laminar flow through a curved tube. *Q. J. Mech. Appl. Math.* (in press).

DE VRIEND, H. J. 1981 Velocity redistribution in curved rectangular channels. *J. Fluid Mech.* **107**, 423–439.

JOSEPH, B., SMITH, E. P. & ADLER, R. J. 1975 Numerical treatment of laminar flow in helically coiled tubes of square cross section. *A.I.Ch.E. J.* **21**, 965–974.

LIN, J. Y. & TARBELL, J. M. 1980 An experimental and numerical study of periodic flow in a curved tube. *J. Fluid Mech.* **100**, 623–638.

MANLAPAZ, R. L. & CHURCHILL, S. W. 1980 Fully developed laminar flow in a helically coiled tube of finite pitch. *Chem. Engng Commun.* **7**, 57–78.

MASLIYAH, J. H. 1980 On laminar flow in curved semicircular ducts. *J. Fluid Mech.* **99**, 469–479.

MASLIYAH, J. H. & NANDAKUMAR, K. 1979 Fully developed viscous flow and heat transfer in curved semi-circular sectors. *A.I.Ch.E. J.* **25**, 478–487.

NANDAKUMAR, K. & MASLIYAH, J. H. 1981 Laminar flow in curved moon-shaped ducts. In *Proc. 2nd Int. Conf. on Numerical Methods in Laminar and Turbulent Flow, Venice* (Ed. C. Taylor & B. A. Schrefler). Pineridge.

NG, M. C. 1980 Steady fully developed flow through a curved tube of circular cross-section. *4th Canadian Symp. on Fluid Dynamics*, Abstract, p. 48.

TARBELL, J. M. & SAMUELS, M. R. 1973 Momentum and heat transfer in helical coils. *Chem. Engng J.* **5**, 117–127.

TRUESDELL, L. C. & ADLER, R. J. 1970 Numerical treatment of fully developed laminar flow in helically coiled tubes. *A.I.Ch.E. J.* **16**, 1010–1015.

VAN DYKE, M. 1978 Extended Stokes series: laminar flow through a loosely coiled pipe. *J. Fluid Mech.* **86**, 129–145.